Available online at www.medicinescience.org

ORIGINAL ARTICLE

Medicine Science International Medical Journal

Medicine Science 2021;10(4):1373-86

Uridine derivatives: Antifungal, PASS outcomes, ADME/T, drug-likeliness, molecular docking and binding energy calculations

Tahmida Shamsuddin[1], Mohammed Anowar Hosen[2], Muhammad Shaiful Alam[3], Talha Bin Emran[4], Sarkar Mohammad Abe Kawsar[2]

[1]University of Chittagong, Faculty of Science, Department of Applied Chemistry and Chemical Engineering, Chittagong, Bangladesh
[2]University of Chittagong, Faculty of Science, Department of Chemistry, Chittagong, Bangladesh
[3]University of Science and Technology Chittagong, Faculty of Basic Medical and Pharmaceutical Sciences, Department of Pharmacy, Chittagong, Bangladesh
[4]BGC Trust University Bangladesh, Department of Pharmacy, Chittagong, Bangladesh

Received 20 May 2021; Accepted 29 June 2021
Available online 24.11.2021 with doi: 10.5455/medscience.2021.05.175

Abstract

Several nucleoside derivatives are used as antifungal, antiviral, antibacterial, and anticancer agents and have shown effective results against fungal, bacteria, viruses, and cancer. In this investigation, we have identified the biological and quantum chemical activities of our previously published synthesized uridine derivatives by in silico approached. The in silico study demonstrated ADME/T (absorption, distribution, metabolism, elimination, toxicity) analysis, drug likeliness test, PASS (prediction of activity spectra for substances) parameter, molecular docking, non-bond interaction, and MM-GBSA (molecular mechanics/generalized born surface area). binding energy calculations. Both the prediction of ADME/T and drug likeliness interpreted for the pharmacokinetics and drug ability of the derivatives. The PASS illustrated that these nucleoside derivatives have shown antifungal and antiviral activity. Besides, molecular docking with a fungal target sterol 14α-demethylase confirmed the antifungal activity that showed a more negative score than two standards, VNI and ampicillin. Compound 7 (5'-*O*-N-acetylsulfanilyl-2′,3′-di-*O*-lauroyluridine) showed the highest docking score (-13.108 kcal/mol), while the parent compound showed the lowest (-6.749 kcal/mol). Non-bonding interaction analysis revealed that compound 7 showed a conventional hydrogen bond with ARG (Arginine) 378, a carbon-hydrogen bond with SER (Serine) 311, a pi-sulfur bond, five alkyl bonds, and four pi-alkyl bonds to the active site. On the other hand, compound 14 [5′-*O*-N-acetylsulfanilyl-2′,3′-di-*O*-(2,6-dichlorobenzoyl)uridine] showed four conventional hydrogen bonds with HIS (Histidine) 310, ARG (Arginine) 378, ILE (Isoleucine) 464, and HIS (Histidine) 461, a carbon-hydrogen bond, two pi-pi-T-shaped, eight alkyl bonds, and seven pi-alkyl bonds with the active site. MM-GBSA binding energy estimation is performed and compared with two standard drugs, VNI and ampicillin.

Keywords: Uridine, drug likeliness, molecular docking, PASS, antifungal, ADME/T

Introduction

Nucleosides are a class of polyhydroxylated compounds that play a pivotal role in metabolism. Consequently, its derivatives have immense contributions in the biotechnology, pharmaceutical, and clinical field as medicinal agents [1-6]. Nucleoside analogs-cytidine 6, thymidine 1,2′-deoxycytidine 2, adenosine 7, and uridine 5 are the building components of RNA or DNA. These derivatives also help to bear genetic information in the cell and transfer it from one to the next generation. Other derivatives such as zidovudine and floxuridine have also been used clinically for antiviral, antifungal, and anticancer activities [1,7-9]. Indeed, cytidine derivative 5-AZA-2′-deoxycytidine has been used to control neuroblastoma malignant tumor growth [10]. In addition to its role as a pyrimidine component of RNA, cytidine has been found to control neuronal-glial glutamate cycling, with supplementation decreasing midfrontal/cerebral glutamate/glutamine levels and cytidine has generated interest as a potential glutamatergic antidepressant drug [11]. Cytidine analogs KP-1461 is an anti-HIV agent that works as a viral mutagen and zebularine exists in *E. coli* and is being examined for chemotherapy [12]. Additionally, several nucleoside derivatives, mildiomycin, AR-12, exhibited potent inhibitory activity against *S. cerevisiae, C. neoformans, and C. albicans* [13-15]. In recent decades, computational chemistry is a popular way to calculate physicochemical, spectral, and biological properties of newly synthesized chemicals [16-25]. So, here fourteen synthesized nucleoside derivatives were computationally investigated to determine their several biological activities. From

***Corresponding Author:** Sarkar Mohammad Abe Kawsar, University of Chittagong, Faculty of Science, Department of Chemistry, Chittagong, Bangladesh
E-mail: akawsar@cu.ac.bd

PASS prediction, we found these derivatives having significant fungal and viral inhibitory activities. So, we have drawn our attention to the study with an emphasis on antifungal activity.

Apart from several targeted modes of action, maximum antifungal drugs have been designed to inhibit sterol 14α-demethylase (CYP5). The main objectives of these drugs are to reduce the amount of ergosterol and accumulation of intermediates in the pathway. Thus, cell membranes are disrupted, resulting in the alteration of numerous membrane-bound enzyme activities [26]. We also set sterol 14α-demethylase as our target protein priority and took VNI and Ampicillin as our reference drugs. In this study, pharmacokinetic prediction has been performed to estimate their absorption, distribution, metabolism, and toxicity to understand the properties of the synthetic compounds. Additionally, these derivatives were optimized to determine their PASS property and biological behavior based on Pa (probability for active molecule) and Pi (probability for inactive molecule) ranges. Molecular docking and MM-GBSA calculations were also discussed to identify the binding mode and binding affinity and nonbonding interaction of nucleoside derivatives with the receptor protein sterol 14α-demethylase.

Materials and Methods

ADME/T analysis and drug-likeliness evaluation

The free web tool pkCSM (predicting small-molecule pharmacokinetic properties using graph-based signatures) [27] was used to evaluate all the pharmacokinetics and physicochemical properties. With the help of these tools that can easily analyze the ADME/T of each ligand. We can also determine the derivatives' applicability as drugs or drug-likeness, lipophilicity, Topological Polar Surface Area (TPSA), bioavailability score, and medicinal chemistry studies by using another online-based tool SwissADME [28]. Before conducting the analysis, with the help of ChemDraw 18.0 software, we have drawn all the structures of our synthetic compounds. The SMILES (simplified molecular-input line-entry system) strings, InChI (International Chemical Identifier) key, SD files were collected from the ChemDraw 18.0 software after drawing. The SMILES strings were used in the pkCSM and SwissADME, while the InChI key was used to search these synthetic compounds in different databases, and SD files were used as input files in molecular docking analysis.

PASS prediction

Online web application PASS (http://www.pharmaexpert.ru/passonline/) has been employed to calculate the antimicrobial activity spectrum of the selected synthetic nucleoside derivatives [29]. This server is planned to surmise above 4000 types of antimicrobial function together with drug and non-drug activity which helps to suggest the best potential objects with 90% validity. PASS outcomes are revealed by Pa (probability for active molecule) and Pi (probability for inactive molecule). Having potentialities, the Pa and Pi scores varies in the range of 0.00 to 1.00 and usually, $Pa + Pi \neq 1$, as these potentialities are predicted freely. The biological actions with $Pa > Pi$ are only thought of as probable for a selected drug molecule. PASS calculation outcomes were explained and used flexibly, viz. (i) when Pa greater than 0.7, the probability to identify the activity is analytically high, (ii) if $0.5 < Pa < 0.7$, the probability to identify the activity is analytically low, again, the molecule is perhaps not so alike to well conversant pharmaceutically used drugs and (iii) if $Pa < 0.5$, the potentiality to identify the activity analytically is less. As a result, prediction of the spectrum of antimicrobial activity of a probable drug molecule is expressed as its intrinsic parameter.

Sterol 14alpha-Demethylase

Cytochrome P450 sterol 14alpha-demethylase is responsible for the biosynthesis of ergosterol. So, by inhibiting it, this is possible to prevent the production of ergosterol, promoting the rapture of the cell membrane in microorganisms [30]. For this reason, we possess docked these synthetic compounds with cytochrome P450 sterol 14α-demethylase to identify the best selective and potential antifungal candidate.

Protein preparation

We retrieved the 3D crystal structure of cytochrome P450 sterol 14α-demethylase from the RCSB protein data bank (PDB ID: 4UYL, organism: *Aspergillus fumigatus*). For molecular docking, the protein structure was prepared using Maestro 11.6 software (Maestro, version 11.6, Schrödinger, LLC). First, we have defined the missing hydrogen atoms, bond orders, charges, disulfide bonds, side chains and removed atomic clashes, metals, and water molecules. We have deleted unwanted chains, water molecules, and het groups from the structure in the refinement process to avoid interaction during the optimization and minimization processes. Then, the hydrogen-bonding networks within the structure were optimized at pH 7.0. After the optimization of H-bonds, the OPLS3e force field was allowed to perform with a specific RMSD value (0.30 Å). Here, we used the OPLS3e force field as it covers about 95% of the molecular interactions during virtual screening. Grid box (18 Å ×18 Å × 18 Å) was made with the default settings using the control ligand to define the active site of the protein [31,32].

Ligand preparation

Ligand preparation is essential to generate the 3D geometries, tautomers, ionization states, chiralities, and precise bond orders. So, after protein preparation, the next step is to prepare the ligand for screening. At first, we drew all the synthetic compound structures and saved them in SDF (structure data file) format. All the ligands were then prepared using LigPrep module 3.1 of Maestro 11.6 software (Maestro, version 11.6, Schrödinger, LLC). We have also used the OPLS3e force field for the optimization at pH 7.0 ± 2.0.

Molecular docking studies

Molecular docking is a fundamental approach for observing the interactions and binding affinity between rigid protein and flexible ligand. All docking simulations were conducted with the Glide module of Maestro 11.6 software (Maestro, version 11.6, Schrödinger, LLC). Then, the OPLS3e force field was used for the complex optimization, and after that, minimization was carried out. Here, we have used VNI – the native ligand of 4UYL and Ampicillin as reference ligands for screening. The charge has been removed, and we have set 0.25 and 1.00 as Van der Waals

scaling factors. It is evident to prefer negative values in docking calculations; a higher negative value identifies a better binding affinity of the protein-ligand complex. We also analyzed the non-bond interaction by Discovery studio software. Here, we have analyzed the best complexes as well as the reference ligand complex to compare the bond type, categories, and active site's residues.

MM-GBSA

MM-GBSA is use for binding affinity analysis and accurate binding conformations determination. In this study, the MM-GBSA module of the Maestro 11.6 software was used. For MM-GBSA calculation, glide XP docking pose viewer (PV) files were used, and sampling minimization protocol was used as a continuum model. As molecular mechanics (MM), the OPLS3e force field was applied to keep the protein flexible. As a dielectric solvent model, VSGB 2.0 was used to modify empirical functions of π-stacking and H-bond interactions. The higher negative value of the protein-ligand complex is referred to as the most stable complex.

Results

The newly modified uridine derivatives were designated according to the reaction scheme (Figure 1).

Table 1 represents the chemical name of the compounds with their molecular formula. After geometrical optimization, all the compounds were subjected to molecular docking and pharmacokinetic prediction.

ADME/T and drug-likeliness analysis

The pharmacokinetic study of 14 compounds was evaluated using the pkCSM online tools and all the findings are given in Table 2.

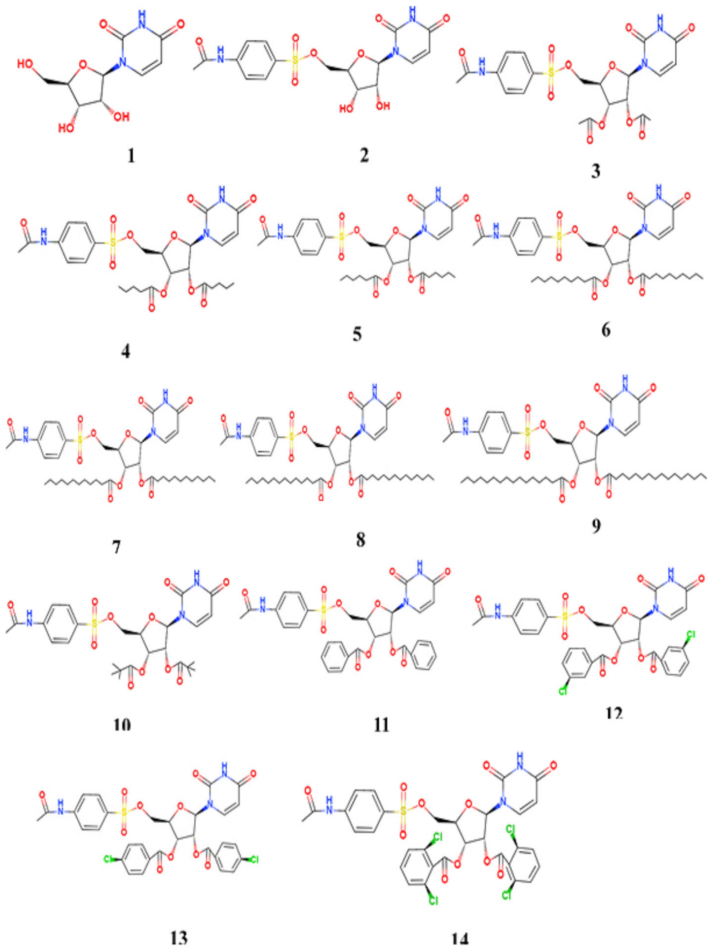

Figure 1. Chemical structure of the uridine (1) and its derivatives (2-14)

Table 1. Molecular formula and name of the designed compounds

Compound	Molecular formula	Name
1	$C_9H_{12}N_2O_6$	Uridine
2	$C_{17}H_{19}N_3O_9S$	5′-*O*-N-acetylsulfanilyluridine
3	$C_{21}H_{23}N_3O_{11}S$	5′-*O*-N-acetylsulfanilyl-2,3′-di-*O*-acetyluridine
4	$C_{27}H_{35}N_3O_{11}S$	5'-*O*-N-acetylsulfanilyl-2',3′-di-*O*-pentanoyluridine
5	$C_{29}H_{39}N_3O_{11}S$	5′-*O*-N-acetylsulfanilyl-2',3′-di-*O*-hexanoyluridine
6	$C_{37}H_{55}N_3O_{11}S$	5′-*O*-N-acetylsulfanilyl-2,′3′-di-*O*-decanoyluridine
7	$C_{41}H_{63}N_3O_{11}S$	5'-*O*-N-acetylsulfanilyl-2′,3′-di-*O*-lauroyluridine
8	$C_{45}H_{73}N_3O_{11}S$	5′-*O*-N-acetylsulfanilyl-2′,3′-di-*O*-myristoyluridine
9	$C_{49}H_{79}N_3O_{11}S$	5′-*O*-N-acetylsulfanilyl-2′,3′-di-*O*-palmitoyluridine
10	$C_{27}H_{35}N_3O_{11}S$	5′-*O*-N-acetylsulfanilyl-2′,3′-di-*O*-pivaloyluridine
11	$C_{31}H_{27}N_3O_{11}S$	5′-*O*-N-acetylsulfanilyl-2′,3′-di-*O*-benzoyluridine
12	$C_{31}H_{25}N_3O_{11}SC_{l2}$	5′-*O*-N-acetylsulfanilyl-2′,3′-di-*O*-(3-chlorobenzoyl)uridine
13	$C_{31}H_{25}N_3O_{11}SC_{l2}$	5′-*O*-N-acetylsulfanilyl-2′,3′-di-*O*-(4-chlorobenzoyl)uridine
14	$C_{31}H_{23}N_3O_{11}SC_{l4}$	5′-*O*-N-acetylsulfanilyl-2′,3′-di-*O*-(2,6-dichlorobenzoyl)uridine

Table 2. ADME/T properties of synthetic compounds by SwissADME

Property	Parameters	1	2	3	4	5	6	7	8	9	10	11	12	13	14	Ampicillin
Physical properties	Molecular Weight	244.203	441.418	525.492	609.654	637.708	749.924	806.032	862.14	918.248	609.654	649.634	718.524	718.524	787.414	349.412
	LogP	-2.8519	-1.4803	-0.3387	2.0019	2.7821	5.9029	7.4633	9.0237	10.5841	1.7137	2.2491	3.5559	3.5559	4.862	0.318
	Rotatable bonds	2	6	8	14	16	24	28	32	36	8	10	10	10	10	4
	H-bond acceptor	7	10	12	12	12	12	12	12	12	12	12	12	12	12	5
	H-bond donor	4	4	2	2	2	2	2	2	2	2	2	2	2	2	3
	Surface area	94.719	169.371	203.792	241.982	254.712	305.631	331.091	356.551	382.011	241.982	261.177	281.783	281.783	302.39	143.121
Absorption	Water solubility	-2.334	-2.265	-3.772	-3.601	-3.724	-3.612	-3.338	-3.11	-2.978	-3.738	-4.115	-4.014	-4.011	-3.869	-2.396
	Caco2 permeability	-0.175	-0.035	-0.063	-0.023	-0.069	-0.292	-0.402	-0.512	-0.622	0.035	0.045	0.055	0.153	0.077	0.395
	Intestinal absorption (human)	43.32	46.679	40.236	60.644	56.389	62.229	65.13	68.032	70.933	64.625	74.887	77.106	77.118	83.861	43.034
	Skin Permeability	-2.796	-2.765	-2.745	-2.736	-2.736	-2.735	-2.735	-2.735	-2.735	-2.736	-2.735	-2.735	-2.735	-2.735	-2.735
	P-glycoprotein substrate	No	Yes	Yes	Yes	Yes	Yes	Yes	Yes	Yes	Yes	Yes	Yes	Yes	Yes	No
	P-glycoprotein I inhibitor	No	No	No	Yes	Yes	Yes	Yes	Yes	Yes	Yes	Yes	Yes	Yes	Yes	No
	P-glycoprotein II inhibitor	No	No	No	No	No	Yes	Yes	Yes	Yes	No	Yes	Yes	Yes	Yes	No

Distribution	VDss (human)	-0.735	-0.805	-0.807	0.081	0.155	0.187	-0.101		-1.071	0.048	-0.449	-0.33	-0.373	-0.344	-1.23
	Fraction unbound (human)	0.978	0.453	0.241	0.178	0.141	0.081	0.098	0.128	0.16	0.1	0	0	0	0	0.752
	BBB permeability	-1.487	-1.996	-2.003	-2.38	-2.432	-2.668	-2.784	-2.901	-3.018	-2.112	-2.102	-2.435		-2.802	-0.767
	CNS permeability	-4.418	-4.104	-3.551	-3.793	-3.66	-3.388	-3.342	-3.295	-3.248	-3.353	-3.999	-3.886	-3.872	-3.784	-3.166
Metabolism	CYP2D6 substrate	No	No	No	No	No	No	No	No	No	No	No	No	No	No	No
	CYP3A4 substrate	No	No	Yes	Yes	Yes	Yes	Yes	Yes	Yes	Yes	Yes	Yes	Yes	Yes	No
	CYP1A2 inhibitor	No	No	No	No	No	No	No	No	No	No	No	No	No	No	No
	CYP2C19 inhibitor	No	No	No	No	No	No	No	No	No	No	No	No	No	No	No
	CYP2C9 inhibitor	No	No	No	No	No	No	No	No	No	No	No	Yes	Yes	Yes	No
	CYP2D6 inhibitor	No	No	No	No	No	No	No	No	No	No	No	No	No	No	No
	CYP3A4 inhibitor	No	No	No	Yes	Yes	Yes	Yes	Yes	Yes	Yes	Yes	Yes	Yes	Yes	No
Excretion	Total Clearance	0.666	0.677	1.115	0.76	0.791	0.908	0.966	0.895	0.952	0.02	0.387	-0.415	-0.541	-0.062	0.337
	Renal OCT2 substrate	No	No	No	No	No	No	No	No	No	No	No	No	No	No	No

Toxicity	AMES toxicity	No	No	No	No	No	No	No	No	No	No	No	No	No	No	No
	Max. tolerated dose (human)	0.878	0.397	0.828	0.024	-0.067	-0.122	0.027	0.201	0.335	-0.194	-0.065	-0.122	-0.126	-0.129	0.952
	hERG I inhibitor	No	No	No	No	No	No	No	No	No	No	No	No	No	No	No
	hERG II inhibitor	No	No	No	No	No	No	No	No	No	No	Yes	Yes	Yes	Yes	No
	Oral Rat Acute Toxicity (LD50)	1.884	2.253	2.307	2.33	2.408	2.561	2.562	2.543	2.52	2.453	2.517	2.497	2.493	2.48	1.637
	Oral Rat Chronic Toxicity (LOAEL)	2.661	2.285	2.234	2.37	2.258	2.723	3.031	3.306	3.475	2.648	2.967	2.882	2.875	2.652	2.398
	Skin Sensitization	No	No	No	No	No	No	No	No	No	No	No	No	No	No	No

Absorption

From Table 2, we could determine the compounds' absorption property based on some features such as water solubility, Caco-2 cell permeability, skin permeability, intestinal absorption of humans, P-glycoprotein substrate, P-glycoprotein I inhibitor, and P-glycoprotein II inhibitor. How a drug is absorbed depends on its water-solubility features. Good water-soluble molecules refer to good absorption properties leading to adequate bioavailability [33]. As indicated in Table 2, compounds 1, 2, 3, 4, 5, 6, 7, 8, 9, 10, and 14 were slightly soluble, while compounds 11, 12, and 13 had higher water-insoluble property, i.e., more soluble in lipid. Caco-2 permeability is another significant parameter that measures a molecule's flux rate across the polarized Caco-2 cell monolayers to predict the absorption of oral drugs from the generated data. A good drug must have a satisfactory Caco-2 permeability [34]. The maximum permeability was found by compounds 13, 10, 11, 12, and 14 had slightly Caco-2 permeability. Higher values of human intestinal absorption are better absorbed on oral administration from GIT [35]. All the compounds displayed higher HIA values ranging from 40.24% to 83.86 %. Skin permeability shows whether the drug molecules can permeable to the skin or not. Here, all fourteen compounds were poorly penetrating to the skin. Both P-glycoprotein I & II inhibitors can increase the bioavailability of susceptible drugs [36]. All compounds from the given table were likely to be a substrate of P-gp except compound 1. Here, compounds 1-3 inhibited the P-glycoprotein I & II, while compounds 4, 5, and 10 only inhibited the P-glycoprotein II and others did not show any interactions.

Distribution

The distributional properties such as VD, fraction unbound, BBB permeability, skin permeability of all compounds are given in Table 2. The drug distribution is directly interlinked with the volume distribution. By volume of distribution (VD), we can predict whether the distribution of a drug between blood and tissue is unformed or not. When the amount of drug in the tissues is higher than the drug concentration in plasma, the VD is higher and can be easily distributed throughout the body. In contrast, lower VD shows higher drug concentration in plasma and can't distribute to the tissues [28] . Here, most of the compounds indicated low VD values, whereas others showed moderate VD values. Another important parameter of drug distribution is the unbound drug fraction in the blood. The bounded drug molecules remained in the plasma and cannot be distributed to the tissues, while the unbound fraction can be easily diffused [37]. Compounds 1, 2, and 3 had shown high fraction unbound values that lead to a good efficacy drug, and the other compounds 4-10 also showed quite satisfactory values of Fu. The blood-brain barrier (BBB) prevents foreign substances' entry into the brain and the central nervous system (CNS). All the compounds shown in the table were unable to permeable to CNS, while they all were poorly permeable to BBB.

Metabolism

After distribution, the drug molecules break down in the liver

through enzymatic reactions. Cytochrome P450, the detoxification enzyme acts as a catalyst for the oxidation of drugs and helps in the drug's metabolic process as well as facilitates excretion [38]. The metabolic properties for the fourteen compounds were evaluated for different isoforms of cytochrome P450 as given in Table 2. Almost all the compounds didn't show any interaction with CYP1A2, CYP2C19, CYP2D6, and CYP2C9 except compounds 12, 13, and 14. In contrast, maximum compounds were metabolized by CYP3A4 excluding compounds 1-3.

Excretion

Drugs are excreted from the body via multiple pathways (kidney, liver, and biliary). Drugs with larger molecular weight (>500) were eliminated from urine, while smaller drug molecules (<300) were excreted from bile. In between 300-500 molecular weights are removed through bile and urine. The excretion of a drug molecule can estimate with the total clearance rate (CLtot). It indicates the amount of drug eliminated per unit time from the combination of hepatic and renal [39]. The CLtot values of all the compounds are mentioned in Table 2. Another essential parameter is Organic Cation Transporter 2 or OCT2 substrate that helps in the renal clearance. Here, no single compound is likely to substrate OCT2.

Toxicity

Unexpected drug toxicity can be a major factor in successful drug candidates' failure and withdrawal of marketed drugs. So, appropriate safety assessment is required for the development and discovery of the drug. It is ensured by predicting several parameters such as - maximum tolerated dose (human), hERG I, II inhibitor, oral rat acute toxicity (LD50), oral rat chronic toxicity (LOAEL), hepatotoxicity, skin sensitization, T. pyriformis toxicity, and minnow toxicity. All the compounds showed no carcinogenicity in AMES toxicity, skin sensitization, and T. pyriformis toxicity. For a successful drug, it is necessary to avoid all interactions with the human ether-a-go-go-gene (hERG) [40]. Compounds 11-14 displayed hERG II inhibitory activity, while none of the compounds inhibited hERG I. After the toxicity assessment, it can be said that most of the compounds were found to have a noncarcinogenic effect (Table 2).

Drug-likeness evaluation

Drug likeness includes a complex balance of all molecular and structural features (molecular weight, lipophilicity, rotatable bonds, surface area, number of hydrogen bond acceptors and donors, bioavailability) by the specific evolution of different computational filters of Lipinski, Ghose, Veber, Egan, and Mueggethe. The entire prediction is described in Table 3. As shown in Table 3, compounds 1 and 2 have minimum violations, and the bioavailability fraction is the same as Ampicillin, while other compounds have shown moderate Bioavailability score.

Table 3. Drug likeness properties of synthetic compounds by PkCSM

Compound	Lipinski violations	Ghose violations	Veber violations	Egan violations	Muegge violations	Bioavailability score
1	0	1	0	0	0	0.55
2	1	1	1	1	1	0.55
3	2	1	2	1	2	0.17
4	2	1	2	1	4	0.17
5	2	3	2	1	4	0.17
6	2	4	2	2	5	0.17
7	2	4	2	2	5	0.17
8	3	4	2	2	5	0.17
9	3	4	2	2	5	0.17
10	2	3	2	1	3	0.17
11	2	3	2	1	3	0.17
12	2	3	2	1	3	0.17
13	2	3	2	1	3	0.17
14	2	3	2	1	3	0.17
Ampicillin	0	0	0	1	0	0.55

PASS analysis

We have predicted the antimicrobial spectrum applying web server PASS (http://www.pharmaexpert.ru/passonline/) of all the synthetic nucleoside derivatives 2–14. The PASS results of yclept as Pa and Pi, are expressed in Table 4. It was manifest from predication Table 6, for synthetic derivatives 2–6 showed $0.29 < Pa < 0.58$ for antibacterial, $0.31 < Pa < 0.61$ for antifungal, $0.41 < Pa < 0.62$ for antiviral and $0.22 < Pa < 0.54$ for anti-carcinogenic. These results revealed that these molecules were more efficient against viruses and fungi in comparison with bacterial pathogens. Attachment of excessive aliphatic and aromatic group increased antifungal activity (Pa ¼ 0.612) of parent (1, Pa ¼ 0.441). The same scenario was observed for antiviral activities. We also tried to predict the anti-carcinogenic parameter of these derivatives. Therefore, PASS determination exhibited $0.22 < Pa < 0.70$ for anti-carcinogenic, which revealed that the synthetic derivatives were less potential as anti-carcinogenic agents than previous antimicrobial parameters. Significantly, synthetic nucleoside derivatives with saturated acyl chains showed more antibacterial, antiviral, and anti-carcinogenic properties comparing with the standard drug ampicillin.

Table 4. Predicted biological activity of the synthetic derivatives using PASS software

	Biological activity							
Compound (Drug)	**Antibacterial**		**Antifungal**		**Antiviral**		**Anti-carcinogenic**	
	Pa	**Pi**	**Pa**	**Pi**	**Pa**	**Pi**	**Pa**	**Pi**
1	0.397	0.031	0.421	0.046	0.627	0.005	0.785	0.006
2	0.299	0.060	0.354	0.013	0.427	0.012	0.339	0.045
3	0.341	0.045	0.401	0.009	0.419	0.012	0.347	0.042
4	0.345	0.039	0.411	0.016	0.423	0.011	0.378	0.031
5	0.331	0.061	0.375	0.024	0.523	0.027	0.705	0.012
6	0.331	0.061	0.375	0.024	0.523	0.027	0.705	0.012
7	0.331	0.061	0.375	0.024	0.523	0.027	0.705	0.012
8	0.331	0.061	0.375	0.024	0.523	0.027	0.705	0.012
9	0.381	0.011	0.415	0.019	0.549	0.011	0.511	0.047
10	0.361	0.059	0.389	0.014	0.511	0.037	0.531	0.039
11	0.246	0.016	0.318	0.017	0.478	0.029	0.365	0.041
12	0.376	0.073	0.497	0.033	0.451	0.062	0.413	0.034
13	0.584	0.003	0.612	0.025	0.624	0.007	0.543	0.037
14	0.509	0.027	0.599	0.051	0.370	0.019	0.224	0.098
Ampicillin	0.750	0.003	0.000	0.000	0.239	0.067	0.000	0.000

Molecular docking

In structural biology and computer aided drug design, molecular docking is an important computational technique. The key aim of molecular docking is to determine the potential binding geometries of a putative ligand of a known three-dimensional structure with a target protein. A total of fourteen synthetic compounds were docked with 14α-sterol demethylase to identify the best ergosterol synthesis inhibitor. The results of their binding energy are given in Table 5. In this study, two reference ligands were used (VNI; PubChem CID: 49867823, and Ampicillin; PubChem CID: 6249). The objective of the study was to evaluate the best synthetic compound that binds better than reference ligands. Here, VNI and Ampicillin's docking scores were -10.24 kcal/mol and -8.6433 kcal/mol, respectively, and VNI exhibited greater affinity to the target than Ampicillin. We know, higher negative values are identified as higher binding affinity, so the potential complex must have a score less than -10.249 kcal /mol.

Almost eight compounds displayed higher binding scores (-13.108 to -10.442 kcal/mol) than VNI. From the Table 5, we found the higher binding affinity in this pattern:7 > 14 > 6 > 13 > 12 > 5 > 4 > 11 > VNI > 2 > 10 > Ampicillin > 3 > 1.

Table 5. Molecular docking (Glide XP) results of synthetic compounds and reference ligands against sterol 14α-demethylase

Compound	Docking score (XP) (kcal/mol)	Glide ligand efficiency (kcal/mol)	Glide energy (kcal/mol)	Glide e-model (kcal/mol)
7	-13.108	-0.234	-74.617	-117.116
14	-12.789	-0.256	-79.286	-129.405
6	-12.652	-0.243	-73.477	-115.128
13	-11.49	-0.239	-70.204	-133.281
12	-11.213	-0.234	-72.065	-133.82
5	-11.014	-0.25	-69.908	-106.253
4	-10.628	-0.253	-71.77	-103.236
11	-10.442	-0.227	-75.185	-121.816
VNI	-8.643	-0.278	-57.187	-83.708
2	-9.088	-0.303	-54.757	-79.244
10	-8.835	-0.21	-67.106	-96.814
Ampicillin	-8.643	-0.332	-43.539	-54.458
3	-8.168	-0.227	-59.065	-93.539
1	-6.749	-0.397	-32.884	-39.428

Nonbonding interactions

The non-bonded interacting amino acids of the target protein, i.e., 14α- sterol demethylase with synthetic compounds, are depicted in Table 6. The standard ligand VNI has shown one conventional hydrogen bond, one carbon-hydrogen bond, two alkyl bonds, and ten pi-alkyl bonds (Figures 2a and 2b). On the other hand, compound 7, possessing the best docking score have exhibited one conventional hydrogen bond with ARG378, one carbon-hydrogen bond with SER311, one pi-sulfur bond with CYS463, five alkyl bonds with CYS463, VAL121, LEU503, VAL135, and LEU143, and four pi-alkyl bonds with TYR122 PHE234 ALA307 ALA469 (Figures 3a and 3b). It has also revealed that compound 14 have five conventional hydrogen bonds with HIS310, ARG378, ILE464, and HIS461, one carbon-hydrogen bond with CYS463, two pi-pi T-shaped bonds with TYR122 and PHE229, eight alkyl bonds with ALA303, ALA307, VAL135, LEU143, LYS147, CYS463, LEU304, and ILE464, and seven pi-alkyl bonds with PHE130, ILE376, VAL135, ALA303, LEU304, ALA307, and CYS463 (Figures 4a and 4b). Compounds 5, 12 and 13 displayed almost equal binding affinity (-11.014, -11.213 and -11.49 kcal / mol) and exhibited some similar binding site with the residues TYR122, HIS310, ARG378 and CYS463. But ARG378 exhibited the shorter distance (1.9018 Å) that indicates tight binding with protein. Compound 7 had two long aliphatic substituent in the uridine structure, providing a high gathering of electrons in the molecule indicated the highest binding score (-13.108 kcal/mol). These results indicated that modification of –OH group along with a long aliphatic chain/aromatic ring molecule increased the binding affinity, while addition of hetero groups like Cl, made some fluctuations in binding affinities; however, modification with halogenated aromatic also rings increased the binding affinity. Nonbonding interactions are often used to predict the shape and behavior of molecules. Among all the non-bonding interactions, CH/O, CH/π, NH/π, OH/π, and CH/N, the CH/O is the highest observed interaction found in protein-ligand docking.

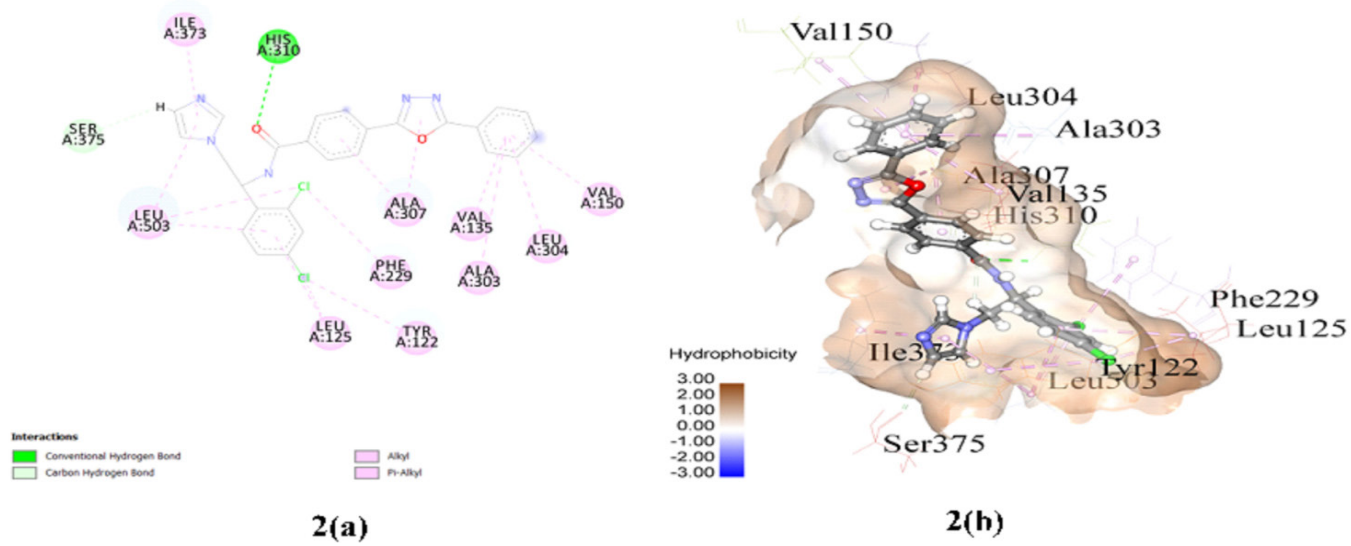

Figure 2. Binding modes of VNI with sterol 14α-demethylase. Molecular interactions are visible on the hydrophobic surface. The binding site of the hydrophobic intensity ranges from −3.00 (minimum hydrophobic region-shade blue) to 3.00 (high hydrophobic region shaded brown). 2(a) 2D view, 2(b) 3D view

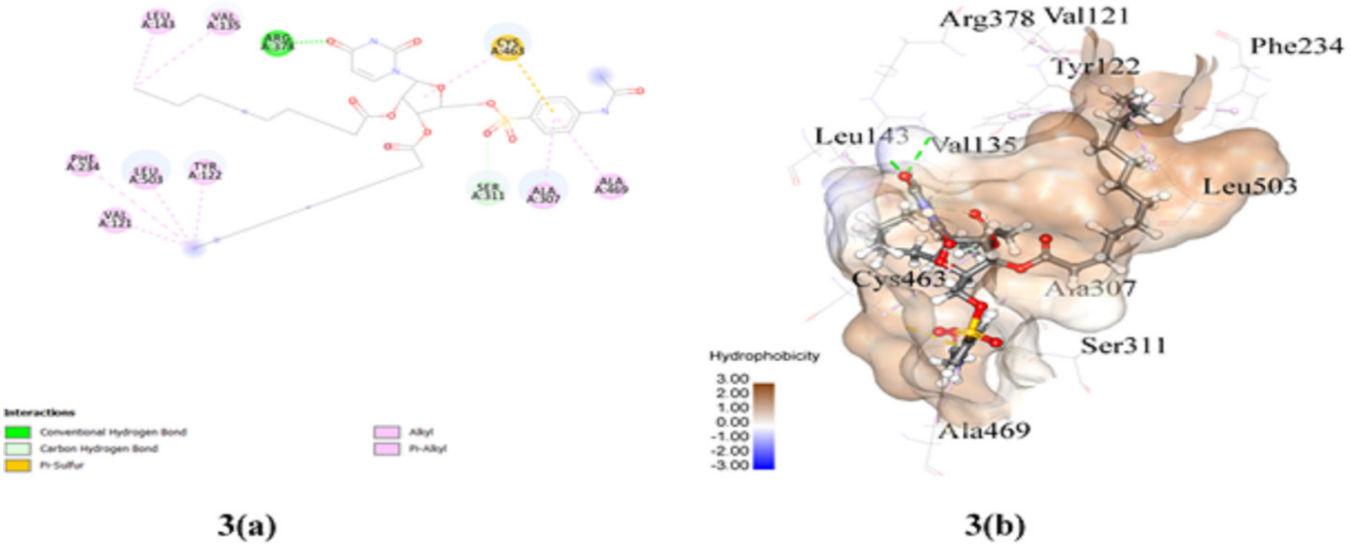

Figure 3. Binding modes of compound 7 with sterol 14α-demethylase. Molecular interactions are visible on the hydrophobic surface. The binding site of the hydrophobic intensity ranges from −3.00 (minimum hydrophobic region-shade blue) to 3.00 (high hydrophobic region shaded brown). 3(a) 2D view, 3(b) 3D view

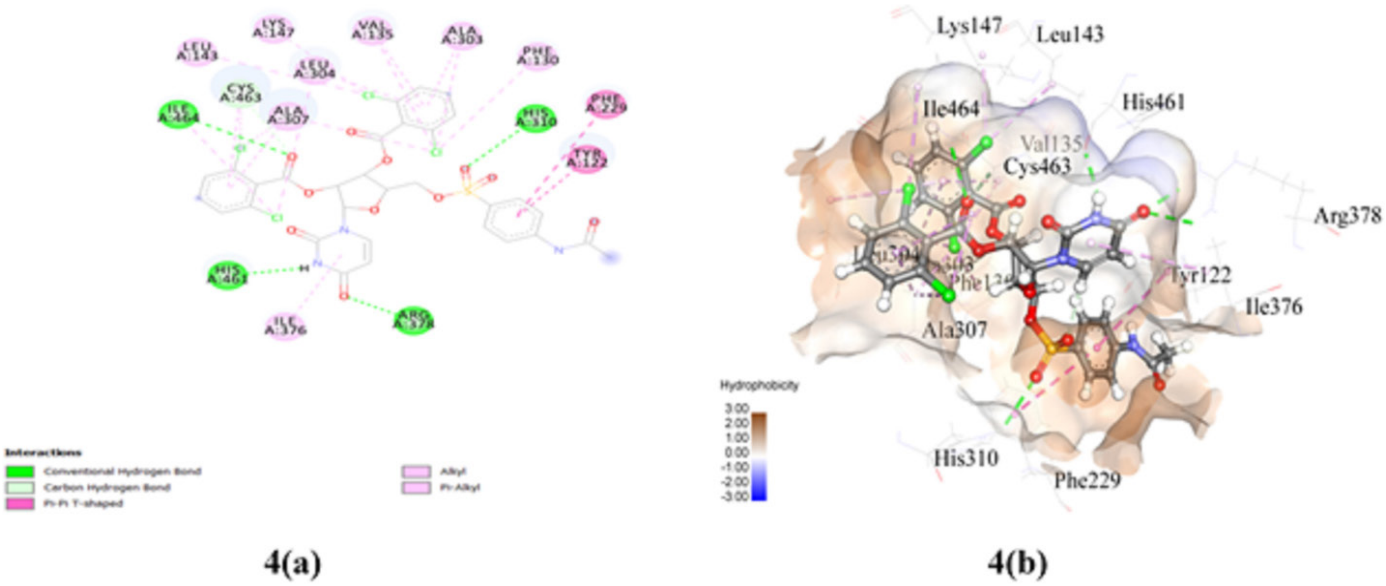

Figure 4. Binding modes of compound 14 with sterol 14α-demethylase. Molecular interactions are visible on the hydrophobic surface. The binding site of the hydrophobic intensity ranges from −3.00 (minimum hydrophobic region-shade blue) to 3.00 (high hydrophobic region shaded brown). 4(a) 2D view, 4(b) 3D view

Table 6. Nonbonding interaction and bond distance (Å) of uridine derivatives and sterol 14α-demethylase complex

Compound	Bond type	Residues and bond distance (Å)
7	**Conventional Hydrogen Bond**	ARG378 (1.62989)
	Carbon Hydrogen Bond	SER311 (2.24922)
	Pi-Sulfur	CYS463 (3.64498)
	Alkyl	CYS463 (5.37084), VAL121 (5.3669), LEU503 (5.06391), VAL135 (4.58026), LEU143 (5.16182)
	Pi-Alkyl	TYR122 (5.11143), PHE234 (5.02232), ALA307 (5.10237), ALA469 (4.95951)
14	**Conventional Hydrogen Bond**	HIS310 (2.72405), ARG378 (2.04949), ILE464 (2.92821), HIS461 (2.12078)
	Carbon Hydrogen Bond	CYS463 (2.54356)
	Pi-Pi T-shaped	TYR122 (4.89615), PHE229 (5.62024)
	Alkyl	ALA303 (3.36316), ALA307 (4.0091), VAL135 (4.64074), LEU143 (5.25398), LYS147 (3.79005), CYS463 (4.04762), LEU304 (4.9458), ILE464 (4.7482)
	Pi-Alkyl	PHE130 (4.3852), ILE376 (5.45512), VAL135 (4.4541), ALA303 (4.68957), LEU304 (5.29138), ALA307 (3.47525), CYS463 (4.95903)
6	**Conventional Hydrogen Bond**	TYR122 (2.47003), ARG378 (1.92801), HIS461 (1.91138)
	Carbon Hydrogen Bond	TYR136 (2.41616)
	Pi-Sigma	TYR122 (2.24267)
	Pi-Pi Stacked	PHE456 (5.00329)
	Alkyl	ALA307 (3.59776), LEU304 (4.99595), LEU125 (4.02452), LEU503 (4.54347)
	Pi-Alkyl	PHE229 (4.94813), ILE373 (5.35714), CYS463 (4.0967), ARG378 (2.72441)
13	**Conventional Hydrogen Bond**	TYR122 (2.08447), HIS310 (2.3672), ARG378 (2.13881)
	Pi-Pi T-shaped	TYR122 (5.35863)
	Alkyl	TYR122 (5.35863), ALA307 (5.04252), VAL150 (4.31513), MET300 (3.57678), LEU304 (3.75349)
	Pi-Alkyl	VAL135 (4.25275), ALA303 (4.38959), LEU304 (5.11869), ALA307 (4.07833), CYS463 (4.80138), ILE464 (5.48464)

12	**Conventional Hydrogen Bond**	ARG378 (1.9018)
	Carbon Hydrogen Bond	TYR122 (3.09393), ALA307 (2.65685), CYS463 (2.55979)
	Pi-Sulfur	PHE130 (5.38227)
	Pi-Pi T-shaped	PHE229 (5.07497)
	Alkyl	ALA303 (3.53229), ALA307 (5.10187), CYS463 (5.17699), VAL135 (4.62541), MET300 (3.74593), LEU304 (4.76411), VAL150 (4.71705), LEU154 (4.83465), LEU304 (4.1858)
	Pi-Alkyl	VAL135 (4.64805), LYS147 (5.43822), VAL150 (5.15176), ALA303 (5.20247), ALA307 (3.97418), CYS463 (5.08458)
5	**Conventional Hydrogen Bond**	HIS310 (2.09451), ARG378 (1.92585), CYS463 (2.00657), HIS461 (2.0652)
	Pi-Sulfur	HIS310 (4.94948)
	Pi-Pi T-shaped	PHE229 (5.14512)
	Alkyl	ALA303 (4.07134), ILE373 (5.21494), VAL135 (4.89089), LEU304 (4.23498)
	Pi-Alkyl	PHE456 (4.07245), ILE376 (5.05673), LEU125 (5.05001), LEU503 (5.16138)
4	**Conventional Hydrogen Bond**	HIS461(1.68102), CYS463 (2.65648), ILE464 (2.57757), GLY465 (2.36228)
	Carbon Hydrogen Bond	ALA307 (2.83218), HIS461 (2.9443), CYS463 (2.36589), ALA303 (2.72067)
	Pi-Donor Hydrogen Bond	TYR122 (3.19377)
	Alkyl	ALA307 (4.14126), VAL135 (4.50775), LEU143 (4.74925), LYS147 (3.86823), LEU205 (4.94239), LEU304 (4.79671)
	Pi-Alkyl	PHE468 (5.29648)
11	**Pi-Pi Stacked**	TYR122 (3.7688)
	Alkyl	ALA307 (3.18236), CYS463 (4.35752), LYS147 (4.01752), LEU143 (3.87291), VAL135 (4.2413), LEU304 (5.42051), ILE464 (4.43915)
	Pi-Alkyl	TYR136 (4.61473), HIS461 (4.6204), ILE373 (4.08185), CYS463 (4.67286)
VNI	**Conventional Hydrogen Bond**	HIS310 (2.43235)
	Carbon Hydrogen Bond	SER375 (2.39818)
	Alkyl	LEU125 (3.51279), LEU503 (4.26114)
	Pi-Alkyl	TYR122 (5.09299), PHE229 (4.53738), ILE373 (4.04787), LEU125 (5.14463), LEU503 (4.84374), ALA307 (3.70445), VAL135 (4.77735), VAL150 (4.83484), ALA303 (4.96222), LEU304 (4.87745)
2	**Conventional Hydrogen Bond**	TYR122 (2.15433), HIS310 (2.28494), ARG378 (2.01488), SER375 (1.84227)
	Carbon Hydrogen Bond	SER375 (2.73715)
	Pi-Sulfur	HIS310 (4.79393)
	Pi-Pi T-shaped	PHE229 (5.09782)
	Pi-Alkyl	ILE373 (5.01289), ILE376 (4.18332), ILE125 (4.98308), LEU503 (5.0038)
10	**Conventional Hydrogen Bond**	TYR136 (2.45217), ILE464 (2.42857), PRO455 (1.98387)
	Carbon Hydrogen Bond	CYS463 (2.46325), TYR136 (2.57237)
Ampicillin	**Salt Bridge; Attractive Charge**	ARG378 (2.01548)
	Conventional Hydrogen Bond	TYR122 (2.20872), TYR136 (1.96537), ARG378 (1.92702), HIS461 (2.13696)
	Carbon Hydrogen Bond	LYS147 (2.84669), HIS461 (2.84144)
	Alkyl	ILE373 (4.2174), ILE376 (4.53165)
	Pi-Alkyl	VAL135 (4.44563), LYS147 (5.31574), VAL150 (5.19812), ALA303 (5.23905), LEU304 (5.49851)
3	**Conventional Hydrogen Bond**	CYS463 (1.98989), ILE464 (2.60775)
	Pi-Pi T-shaped	TYR122 (5.02019)
	Alkyl	ALA307 (3.82298)
	Pi-Alkyl	VAL135 (4.44802), VAL150 (5.27408), ALA303 (4.98228), LEU304 (5.28465)
1	**Conventional Hydrogen Bond**	HIS310 (2.20812), SER375 (1.82863)
	Pi-Pi T-shaped	PHE229 (5.51196)
	Pi-Alkyl	LEU125 (4.93922), LEU503 (5.24387)

N.B. TYR = Tyrosine, CYS = Cysteine, HIS = Histidine, ARG = Arginine, LEU = Leucine, MET = Methionine, VAL = Valine, ALA = Alanin, PHE = Phenylalaine, PRO = Proline, LYS = Lysine, ILE = Isoleucine, SER = Serine

Compounds 2 and 3 that are modified by smaller carbon chain exhibited comparatively lower binding score (-9.088 and -8.168 kcal/mol) due to liter density of electron. Again compound 4 showed a little bit better score (-10.628 kcal/mol) due to having slightly longer carbon chain. Along with PHE229, most of the compounds displayed the maximum π- π interactions with the denoting the tight binding with the active site. Reports suggest that PHE229 is considered as the principal component of the PPS and PPT responsible for the accessibility of small molecules to the active site. In both cases, binding affinity and binding specialty are increased in case of compound (4-7) and (11-14) due to significant hydrogen bonding. It was observed that modifications of –OH group of uridine (1) increased the π-π interactions with the residues of the active site, while increasing their polarity resulted in the formation of hydrogen bonding interactions. The most significant H-bonds were obtained for the compound (2, 4, 5, 6, 13 and 14), forming with HIS310, TYR122 and ARG378 residues. It has already been reported that ten commercial medicines possibly form H-bonds with key residues of macromolecule. H-bonds executed a vital function in shaping the specificity of ligand binding with the receptor, drug design in chemical and biological processes, and molecular recognition and biological activity. Through this non-bond interaction study, also we analyze the bonding distance. To evaluate the stability of these compounds we further analyzed their binding free energy through MM-GBSA methods. From Table 6, we found that almost compounds 14, 6, 13, 5, 4, 2, and 10 bind in the same active site of 4UYL as VNI and showed more conventional hydrogen bonding than VNI.

MM-GBSA

The free energies of target-ligand complexes can be analyzed from the following Table 7. Here, the higher the negative value means that the affinity of the binding is greater. It was found that the binding affinity of the reference ligands VNI and Ampicillin were -83.93 kcal/mol and -54.89 kcal/mol, respectively. Herein, Ampicillin showed quite unsatisfactory free energy value compared to other target-ligand complexes. Most of the compounds exhibit relatively good binding affinity as VNI. The free energy value of compound 13 was the closest to the reference ligand value.

Table 7. MM-GBSA Binding affinity calculation of sterol 14α-demethylase and synthetic compounds complexes

Compounds	ΔG_{Bind} [a]	ΔG_{Bind} Coulomb[b]	ΔG_{Bind} Covalent[c]	ΔG_{Bind} Hbond[d]	ΔG_{Bind} Lipo[e]	ΔG_{Bind} SolvGB[f]	$\Delta G_{BindvdW}$ [g]
VNI	-83.93	110.51	3.6	-0.6	-40.76	-94.45	-58.9
13	-81.99	-6.59	-1.55	-1.73	-26.46	22.4	-67.13
12	-79.3	-1.76	7.09	-0.2	-27.11	22.05	-79.37
14	-78.41	-17.5	4.74	-1.32	-27.52	33.27	-69.47
11	-77.87	-4.98	2.67	-1.18	-23.22	21.91	-72.42
5	-75.7	-14.68	11.93	-1.54	-25.55	24.56	-71.48
4	-73.07	-14.18	10.59	-1.71	-23.97	23.38	-67.01
7	-72.7	-13.39	9.21	-1.57	-36.93	38.59	-68.41
6	-67.34	-29.03	13.74	-2.22	-30.44	49.53	-68.01
3	-63.18	-4.78	3.37	-0.4	-15.58	15.33	-60.56
10	-61.26	-10.14	6.69	-2.21	-18.82	23.63	-61.7
Ampicillin	-54.89	-88.7	3.87	-3.43	-14.5	88.39	-40.52
2	-53.05	-23.11	4.16	-2.3	-11.67	20.86	-33.75
1	-29.42	-8.1	5.52	-1.15	-10.41	14.35	-27.99

[a]MM-GBSA free energy (kcal/mol) of binding.
[b]Contribution to the MMGBSA affinity of binding (kcal/mol) from the Coulomb energy.
[c]Contribution to the MMGBSA affinity of binding (kcal/mol) from covalent binding.
[d]Contribution to the MMGBSA affinity of binding (kcal/mol) from hydrogen bonding.
[e]Contribution to the MMGBSA affinity of binding (kcal/mol) from lipophilic binding.
[f]Contribution to the MMGBSA affinity of binding (kcal/mol) from the generalized Born electrostatic solvation energy.
[g]Contribution to the MMGBSA affinity of binding (kcal/mol) from the van der Waals energy.

Discussion

The investigation of the fourteen synthesized antifungal uridine derivatives (Figure 1) was conducted through computational methods. For this, we have performed ADME/T prediction, PASS analysis, molecular docking, non-bonding interaction, and finally, MM-GBSA analysis. The ADME/T and drug-likeness evolution have given us detailed information about these fourteen compounds along with Ampicillin [8]. We observed that compounds 1, 2 retained the desired physical properties (molecular weight, LogP, rotatable bonds, H-bond acceptor, H-bond donor, and surface area), while others not found to be as expected results [32]. In

the absorption portion, compounds 1-10 and 14 had a slightly water-soluble property with higher intestinal absorption values. Very low BBB permeability and non-permeable CNS properties were exhibited by all synthesized compounds, indicating good distribution property. Most of the compounds (1-11) did not interact with the isozymes of cytochrome P450. Besides, all compounds have acceptable excretion properties without any toxic effect. Among all, compounds 1, 2 were observed as the best candidate compound similar to the reference one and they also showed minimal violations [15].

After having the satisfactory result of ADME/T and drug-likeness features, we analyzed the PASS ranges of all compounds and Ampicillin via an online web server. The findings have revealed that the synthetic compounds were more effective towards antifungal, antiviral parameters than the antimicrobial or anticarcinogenic parameters. Based on the PASS results, we proceeded with our work of these examined synthesized constituents against the viral activity [30]. It has been found that compounds 5, 6, 7, 9, 11, 13, and 14 showed an excellent result, that very much close to Ampicillin value. The compounds were sorted in Table 5 according to their higher docking score. Here, several compounds (7, 14, 6, 13, 12, 5, 4, and 11) had greater binding affinities than VNI and Ampicillin. Interestingly, we got VNI had a higher affinity compared to Ampicillin. Among all, compounds 7 and 14 were the best bidders with the highest docking scores -13.108 and -12.789 kcal/mol, respectively. In contrast, the lowest scores were -8.168 and -6.749 kcal/mol for compounds 3 and 1.

Here, we also compared the non-bonding interaction of 14α-sterol demethylase with VNI and the best-synthesized compounds based on the docking score [30]. It was admittedly visible that compound 14 had more conventional bonds in comparison to compound 7, indicating its strong binding affinity with 14α- sterol demethylase. Additionally, an increased number of conventional hydrogen bonds in compounds 14, 6, 13, 5, 4, 2, and 10 than VNI, refer to the inhibitory potential of our target protein. We analyzed the bonding distance for each synthesized component. MM-GBSA score was also estimated to determine the affinity of the 14 synthesized compounds and the two reference drugs (VNI and Ampicillin) towards 14α- sterol demethylase. The result found compounds 13, 12, and 14 were highly stable than Ampicillin and nearly to VNI. From the overall analysis of docking and MM-GBSA calculation, we can propose that compounds 12, 13, and 14 can be excellent potential 14α-sterol demethylase inhibitors. In vitro and in vivo investigations are further recommended to confirm the molecular docking and MM-GBSA results.

Conclusion

In this investigation, the inherent characteristic stability and biochemical behavior of synthesized nucleoside derivatives have been studied. We investigate the ADME/T properties of these 14 synthesized nucleoside derivatives with the standard drug ampicillin to know their potential to be like a drug in the future. We predicted the PASS properties to identify the optimal efficacy of the biological activities of these compounds. PASS prediction of the uridine derivatives 1–14 was $0.29 < Pa < 0.58$ for antibacterial, $0.31 < Pa < 0.61$ for antifungal, $0.41 < Pa < 0.62$ for antiviral and $0.22 < Pa < 0.54$ for anti-carcinogenic. Based on the Pa and Pi value, we have come to a decision that the synthesized nucleoside derivatives exhibited the best antifungal and antiviral potency, and proceeded against fungi activities with these synthetic compounds. For further assessment, virtual screening, nonbonding interaction, and MM-GBSA were performed and compared with VNI and ampicillin values. By combining the docking and MM-GBSA analysis, we can state that compounds 12, 13, and 14 were the best bidders among all. This study concluded that these three synthesized nucleoside derivatives were effective against 14α-sterol demethylase inhibitor, still further development and in vitro and in vivo analyses are mandatory for future.

Conflict of interests
The authors declare that they have no competing interests.

Financial Disclosure
All authors declare no financial support.

Ethical approval
No ethical approval is needed for this research.

References

1. Clercq DE. Antiviral drugs in current clinical use. J Clin Virol. 2004:30;115–133.
2. Bulbul MZH, Chowdhury TS, Misbah MMH, et al. Synthesis of new series of pyrimidine nucleoside derivatives bearing the acyl moieties as potential antimicrobial agent. Pharmacia. 2021:68;23–34.
3. Maowa J, Alam A, Rana KM, et al. Synthesis, characterization, synergistic antimicrobial properties and molecular docking of sugar modified uridine derivatives. Ovidius Univ Ann Chem. 2021:32;6–21.
4. Kawsar SMA, Hamida AA, Sheikh AU, et al. Chemically modified uridine molecules incorporating acyl residues to enhance antibacterial and cytotoxic activities. Int J Org Chem. 2015:5;232–45.
5. Arifuzzaman M, Islam MM, Rahman MM, et al. An efficient approach to the synthesis of thymidine derivatives containing various acyl groups: characterization and antibacterial activities. ACTA Pharm Sci. 2018:56;7-22.
6. Kawsar SMA, Kabir AKMS, Matin MM, et al. Synthesis and antibacterial activities of some uridine derivatives. Ctg Univ J Sci. 1998:22;13-8.
7. Clercq DE, Field, HJ. Antiviral prodrugs–the development of successful prodrug strategies for antiviral chemotherapy. British J Pharmacol. 2006:147;1–11.
8. Devi SR, Jesmin S, Rahman M, et al. Microbial efficacy and two step synthesis of uridine derivatives with spectral characterization. ACTA Pharm Sci. 2019:57;47–68.
9. Maowa J, Hosen MA, Alam A, et al. Pharmacokinetics and molecular docking studies of uridine derivatives as SARS- COV-2 Mpro inhibitors. Phy Chem Res. 2021:9;385–412.
10. Gowher H, Jeltsch A. Mechanism of inhibition of DNA methyltransferases by cytidine analogs in cancer therapy. Cancer Biol Therapy. 2004:3;1062–8.
11. Yoon SJ, Lyoo IK, Haws C, et al. Decreased glutamate/glutamine levels may mediate cytidine's efficacy in treating bipolar depression: a longitudinal proton magnetic resonance spectroscopy study. Neuropsychopharmacology. 2009:34;1810–8.
12. Harris K, Sergueev D, Reno J. The chemistry and biology of KP-1461, a selective nucleoside mutagen for HIV therapy. Retrovirology. 2006:3;1–1.
13. Harada S, Mizuta E, Kishi T. Structure of mildiomycin, a new antifungal nucleoside antibiotic. J Am Chem Soc. 1978:100;4895–7.
14. Koselny K, Green J, Favazzo L, et al. Antitumor/antifungal celecoxib derivative AR-12 is a non-nucleoside inhibitor of the ANL-family adenylating enzyme acetyl CoA synthetase. ACS Infect Diseases. 2016:2;268–80.
15. Bulbul MZH, Hosen MA, Ferdous J, et al. Thermochemical, DFT study, physicochemical, molecular docking and ADMET predictions of some modified uridine derivatives. Int J New Chem. 2021:8;88–110.

16. Manly CJ, Louise-May S, Hammer JD. The impact of informatics and computational chemistry on synthesis and screening. Drug Discov Today. 2001:6;1101–10.

17. Kawsar SMA, Islam M, Jesmin S, et al. Evaluation of the antimicrobial activity and cytotoxic effect of some uridine derivatives. Int J Biosci. 2018:12;211–9.

18. Shagir AC, Bhuiyan MMR, Ozeki Y, et al, Simple and rapid synthesis of some nucleoside derivatives: structural and spectral characterization. Curr Chem Lett. 2016:5;83–92.

19. Mirajul MI, Arifuzzaman M, Monjur MR, et al. Novel methyl 4,6-O-benzylidene-α-D-glucopyranoside derivatives: synthesis, structural characterization and evaluation of antibacterial activities. Hacettepe J Biol Chem. 2019:47:153–64.

20. Kawsar SMA, Hasan T, Chowdhury SA, et al. Synthesis, spectroscopic characterization and in vitro antibacterial screening of some D-glucose derivatives. Int J pure App Chem. 2013:8;125-35.

21. Misbah MMH, Ferdous J, Bulbul MZH, et al, Evaluation of MIC, MBC, MFC and anticancer activities of acylated methyl β-D-galactopyranoside esters. Int J Biosci. 2020:16;299–309.

22. Alam A, Hosen MA, Islam M, et al. Synthesis, Antibacterial and cytotoxicity assessment of modified uridine molecules. Curr Adv Chem Biochem. 2021:6;114-29.

23. Kawsar SMA, Kumar A. Computational investigation of methyl α-D-glucopyranoside derivatives as inhibitor against bacteria, fungi and COVID-19 (SARS-2). J Chil Chem Soc. 2021:66;5206-14.

24. Rana KM, Ferdous J, Hosen A, et al. Ribose moieties acylation and characterization of some cytidine analogs. J Sib Fed Univ Chem. 2020:13;465–78.

25. Kawsar SMA, Hosen MA, Fujii Y, et al. Thermochemical, DFT, molecular docking and pharmacokinetic studies of methyl β–D-galactopyranoside esters. J Comput Chem Mol Model. 2020:4;452–62.

26. Lepesheva GI, Ott RD, Hargrove TY, et al. Sterol 14α-demethylase as a potential target for antitrypanosomal therapy: enzyme inhibition and parasite cell growth. Chem Biol. 2007:14;1283–93.

27. Pires DE, Blundell TL, Ascher DB. pkCSM: predicting small-molecule pharmacokinetic and toxicity properties using graph-based signatures. J Med Chem. 2015:58;4066–72.

28. Daina A, Michielin O, Zoete V. SwissADME: a free web tool to evaluate pharmacokinetics, drug-likeness and medicinal chemistry friendliness of small molecules. Scientific Report. 2017:7;1–13.

29. Lagunin A, Stepanchikova A, Filimonov D, et al. PASS: prediction of activity spectra for biologically active substances. Bioinformatics. 2000:16;747–8.

30. Farhana Y, Amin MR, Hosen MA, et al, Monosaccharide derivatives: synthesis, antimicrobial, pass, antiviral, and molecular docking studies against sars-cov-2 mpro inhibitors. J Cell Chem Technol. 2021: In press.

31. Kawsar SMA, Hosen MA. An optimization and pharmacokinetic studies of some thymidine derivatives. Turk Comput Theor Chem. 2020:4;59–66.

32. Alam A, Hosen MA, Hosen A, et al. Synthesis, characterization, and molecular docking against a receptor protein FimH of Escherichia coli (4XO8) of thymidine derivatives. J Mex Chem Soc. 2021:65;256–76.

33. Xu W, Ling P, Zhang T. Polymeric micelles, a promising drug delivery system to enhance bioavailability of poorly water-soluble drugs. J Drug Delivery. 2013:340315.

34. Vishvakarma VK, Nand B, Kumar V, et al. Xanthene based hybrid analogues to inhibit protease of novel corona Virus: Molecular docking and ADMET studies. Comput Toxicol. 2020:16;100140.

35. Nainwal LM, Shaququzzaman M, Akhter M, et al. Synthesis, ADMET prediction and reverse screening study of 3, 4, 5-trimethoxy phenyl ring pendant sulfur-containing cyanopyrimidine derivatives as promising apoptosis inducing anticancer agents. Bioorg Chem. 2020:104;104282.

36. Finch A, Pillans P. P-glycoprotein and its role in drug-drug interactions. Aust Prescr. 2014:37;137–9.

37. Kok-Yong S, Lawrence L, Ahmed T. Drug distribution and drug elimination. Basic pharmacokinetic concepts and some clinical applications. Intechopen, 2015. 99–116.

38. McDonnell AM, Dang CH. Basic review of the cytochrome p450 system. J Adv Pract Oncol. 2013:4;263–8.

39. Dowd FJ, Johnson B, Mariotti A. Pharmacology and therapeutics for dentistry-E-Book: Elsevier Health Sciences, 2016.

40. Garrido A, Lepailleur A, Mignani SM, et al. hERG toxicity assessment: useful guidelines for drug design. European J Med Chem. 2020:195;112290.